Eur. Phys. J. E (2008)
DOI 10.1140/epje/i2008-10389-0

THE EUROPEAN PHYSICAL JOURNAL E

The role of the amorphous phase in the re-crystallization process of cold-crystallized poly(ethylene terephthalate)

M. Pieruccini[1,a], A. Flores[2], U. Nöchel[3], G. Di Marco[1], N. Stribeck[3], and F.J. Baltá Calleja[2]

[1] CNR, Istituto per i Processi Chimico-Fisici, Messina, Salita Sperone Contrada Papardo, sn I-98158 Faro Superiore, Messina, Italy
[2] Instituto de Estructura de la Materia, CSIC, Serrano 119, 28006 Madrid, Spain
[3] Institut für Technische und Makromolekulare Chemie, Universität Hamburg, Hamburg, Germany

Received 10 June 2008
Published online: 18 November 2008 –

Abstract. The process of re-crystallization in poly(ethylene terephthalate) is studied by means of X-ray diffraction (SAXS and WAXS) and dynamical mechanical thermal analysis. Samples cold-crystallized for 9 h at the temperatures $T_c = 100\,^{\circ}\mathrm{C}$ and $T_c = 160\,^{\circ}\mathrm{C}$, *i.e.* in the middle of the α relaxation region and close to its upper bound, respectively, are analyzed. During heating from room temperature, a structural rearrangement of the stacks is always found at $T_r \simeq T_c + 20\,^{\circ}\mathrm{C}$. This process is characterized by a decrease of the linear crystallinity, irrespective of T_c; on the other hand, the WAXS crystallinity never increases with T below $T_c + 30\,^{\circ}\mathrm{C}$. The lamellar thickness in the low-T_c sample decreases significantly after the structural transition, whereas in the high-T_c sample the lamellar thickness remains almost unchanged. In both, high- and low-T_c, the interlamellar thickness increases above T_r. Moreover, the high-T_c sample shows a lower rate of decrease of the mechanical performance with increasing T as the threshold T_r is crossed. This result is interpreted in terms of the formation of rigid amorphous domains where the chains are partially oriented. The presence of these domains would determine i) the stabilization of the crystalline lamellae from the thermodynamic point of view and ii) the increase of the elastic modulus of the amorphous interlamellar regions. This idea is discussed by resorting to a phase diagram. An estimation of the chemical-potential increase of the interlamellar amorphous regions, due to the enhancement of the structural constraints hindering segmental mobility, is offered. Finally, previous calculations developed within the framework of the Gaussian chain model (F.J. Baltá Calleja *et al.*, Phys. Rev. B **75**, 224201 (2007)) are used here to estimate the degree of chain orientation induced by the structural transition of the stacks.

PACS. 61.41.+e Polymers, elastomers, and plastics – 61.05.cp X-ray diffraction – 64.70.Nd Structural transitions in nanoscale materials

1 Introduction

When high-molecular-weight polymers crystallize from either the melt or the glass, never reach a complete crystallinity. Entanglements, chain torsions and other conformational defects are pushed towards the core of the amorphous regions by the growing crystals' fronts. Due to chain connectivity, these defects eventually prevent local chain re-adjustments for the further accommodation of segments into the crystalline cells.

Since chain conformational fluctuations are accompanied by corresponding density fluctuations (see, for instance, Doi and Edwards [1]), the mechanism that hinders crystallization at the late stages of growth can be described in terms of confinement effects in the density fluctuation spectrum of the amorphous regions. This viewpoint has been recently used in the description of the high-temperature vitrification process occurring in cold-drawn poly(ethylene terephthalate) (PET) in the course of cold-crystallization at temperatures below 140 °C [2]. The same ideas find application in the interpretation of the multiple α-process in semicrystalline PET [3].

The general scheme outlined above can be expressed in terms of statistical mechanics through the partition function associated to the density fluctuations in a polymeric liquid. Let Z_0 be the partition function in a system where all the density normal modes (*i.e.* plane waves) are free to fluctuate, with the energy distribution among the modes conforming to thermal equilibrium. The presence of constraints can be envisaged as the "quenching" of certain modes, the fluctuation spectrum being described in this case by a partition function $Z_q < Z_0$. A density fluctuation, and a corresponding conformational rearrangement, may occur provided the fluctuation itself has a free energy

[a] e-mail: pieruccini@me.cnr.it

F larger than the barrier [2,3]

$$\Delta F \equiv -k_{\mathrm{B}}T \ln \frac{Z_q}{Z_0}\,. \tag{1}$$

This approach is similar to Adam and Gibbs [4] viewpoint for the description of liquids close to their glass transition temperature, T_g. In the latter case, the constraints to the conformational rearrangements are meant to be of a somewhat different nature, that is, the long-wavelength modes become so slow on approaching the glass transition (from above) that they appear like quenched (in this sense we may call this a *kinetic confinement*). As the temperature decreases, cooperative motions of ever increasing characteristic length are requested for structural rearrangements, leading eventually to a glassy state. The interesting point of the Adam-Gibbs concept is that it may be used to describe the course of the late stages of crystallization in polymers. However, in this case the mode quenching is not caused by slow kinetics but rather by the presence of immobile crystalline domains. In this way, one may describe the fact that confinement of the amorphous phase hinders crystal growth by using statistical mechanical concepts and opening at the possibility of a thermodynamic description of this phenomenology. Hence, the density (conformational) fluctuation dynamics has a central role in this attempt.

A number of processes in polymer science, which involve the evolution of metastable states, may be approached following this idea. Among them, the mechanisms of re-crystallization, multiple melting and those associated with the formation of a Rigid Amorphous Phase (RAP) —or in general, of a non-crystalline phase with lower mobility than the ordinary amorphous phase— are still matter of debate [5–9]. Within this context, for example, secondary crystallization plays a fundamental role in constructing models for the interpretation of the experimental data.

The process of melting and re-crystallization has been recently discussed on the basis of structural (small- and wide-angle X-ray scattering, SAXS and WAXS, respectively) and calorimetric data obtained during heating at different rates of samples previously isothermally cold-crystallized at various temperatures [5].

In the present study we focus on some aspects of the re-crystallization process reported in the preceding article [5] and discuss some of the data reported there in the light of new results from dynamical mechanical thermal analysis (DMTA) and SAXS. We offer a possible interpretation of these results in terms of well-established concepts relating to the thermodynamics of liquids close to their glass transition, *i.e.* from the above outlined point of view. The aim of this paper is to introduce further ideas to complement the existing schemes currently available for the interpretation of the re-crystallization process.

2 Experimental

Glassy PET from Goodfellow (ES 301465) in form of films of 0.5 mm thickness was used; the molecular weight is $M_w \sim 20000\,\mathrm{g/mol}$. Samples were crystallized at the temperatures of 100 and 160 °C for 9 h under nitrogen before the experiments were carried out.

The DMTA was carried out by means of a Polymer Laboratories MKII analyzer. The mechanical behavior of cold-crystallized PET samples ($T_c = 100$ and 160 °C) was followed from 50 to 200 °C at a heating rate of 2 °C/min and an accuracy of 0.1 °C; the probing frequencies were 0.3 and 3 Hz.

The SAXS patterns were recorded using the synchrotron radiation source at DESY, HASYLAB (beamline A2), with a wavelength of $\lambda = 1.50$ Å. A mar CCD camera placed at 294 cm from the sample was used. The centre of the primary beam was displaced to the bottom of the detector, in order to record the scattered intensity, $I(s)$, over a wide range of scattering vector values, s ($s = 2\sin 2\theta/\lambda$, $0.02 \leq s \leq 0.3\,\mathrm{nm}^{-1}$, where 2θ is the scattering angle). Experiments were carried out under two different conditions: A) during a heating cycle similar to that of the DMTA experiments, for $T_c = 160$ °C (high-T_c sample) and B) isothermally, as a function of time, at the temperatures of i) 115 and 125 °C for $T_c = 100$ °C (low-T_c samples) and ii) 175 and 185 °C for the high-T_c samples.

The intensity distribution scans as a function of s were obtained from the azimuthal integration of the two-dimensional SAXS patterns. Calibration against a rat tendon tail standard was accomplished. The intensity values were corrected for the beam intensity and the background scattering was subtracted.

The average values of the crystalline, l_c, and amorphous, l_a, layer thicknesses of the cold-crystallized samples were obtained from the Interface Distribution Function (IDF) $g_1(r)$ [10]. The latter is derived from the one-dimensional Fourier transform of the interference function $G_1(s)$ of the two-phase system, following [11]:

$$g_1(r) = 2\int_{\infty}^{0} G_1(s)\cos(2\pi s r)\mathrm{d}s. \tag{2}$$

The computation of $G_1(s)$ from the scattering intensity $I(s)$ is described elsewhere [5]. The $g_1(r)$ function is proportional to the second derivative of the correlation function and represents the probability of finding interfaces between a crystal and the adjacent amorphous region at a distance r.

The IDFs were fitted to various statistical models that describe the arrangement of the crystalline lamellae. One of the two following models was found to best fit the $g_1(r)$ functions: i) a classical model of infinite paracrystalline stacking [12] and ii) a model of coupled finite paracrystalline stacks [13]. In the former model, l_c was attributed to the lamellar thickness with the smallest relative variance; in the latter one, l_c and l_a are univocally determined. The average l_c and l_a values were derived from the model which was found to better fit the data. All data obtained at long crystallization times (> 50 min) in the isothermal experiments (B-type), as well as those of the $T_c = 160$ °C sample during heating (A-type), were analyzed with the same model (infinite paracrystalline stacking).

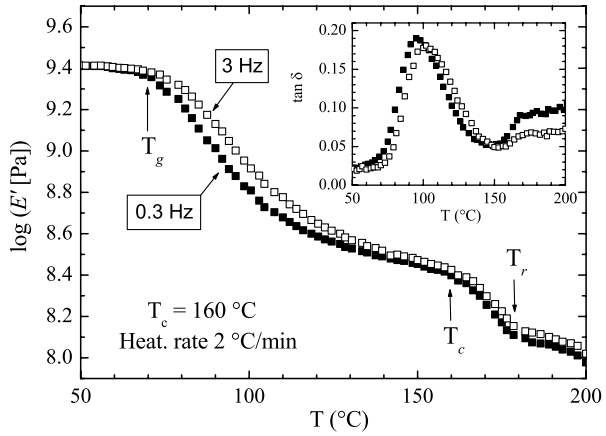

Fig. 1. Logarithm of the storage modulus E' at 0.3 and 3 Hz obtained with a heating rate of 2 °C/min on cold-crystallized PET annealed at the temperature $T_c = 160$ °C for 9 h. The vertical arrows indicate the relevant temperatures in the heating process: T_g (glass transition), T_c (crystallization) and T_r (re-crystallization). The inset shows the corresponding loss tangent patterns.

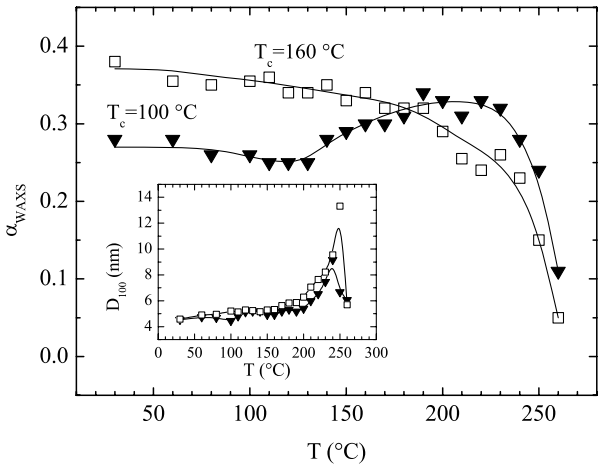

Fig. 2. WAXS crystallinity as a function of the temperature during a heating run at a rate of 2 °C/min for PET samples crystallized at 100 and 160 °C for 9 h. The inset reports the corresponding values of the coherence length D_{100}; symbols correspond to those of the main frame. The data are taken from reference [5].

3 DMTA and X-ray scattering results

3.1 High-T_c sample

Figure 1 shows the real part of the dynamic modulus, E', at two different frequencies, as a function of the increasing temperature T, for the sample crystallized at 160 °C. The relaxation process associated to the significant decrease of E' in the temperature range between ~ 70 and ~ 140 °C is also revealed by a peak in the corresponding loss tangent patterns included in the inset. This corresponds to the α-transition, whose kinetic character is demonstrated by the frequency dependence of the peak position. The rather wide temperature interval over which this process takes place is a result of the diversity of the non-crystalline regions: a) those sandwiched between lamellae within the stacks, which should be responsible of the high-T tail of the dispersion region and b) the inter-stack amorphous pockets, which should mainly contribute to the low-T part of the spectrum (cf. also Ref. [3]).

In preceding calorimetric studies, it has been shown that a number of polymers crystallized isothermally at a given T_c during a certain time t, show a first endothermal peak at a "re-crystallization" temperature, T_r, larger than T_c [6]; the difference $T_r - T_c$ increases with increasing crystallization time t. In the case of PET this difference reaches values of about 20 °C, almost independent of T_c, for the crystallization times imposed to our samples (cf. also Ref. [14] for a thorough account).

It is to be noted that as T crosses the crystallization temperature T_c in our DMTA, the weakening rate of the modulus increases until a discontinuity in $|\mathrm{d} \log E'/\mathrm{d}T|$ is encountered. The temperature where this discontinuity is found practically coincides with T_r and does not depend significantly on the probing frequency, which denotes the thermodynamic (and not kinetic) nature of the underlying process. The same behaviour can be observed more clearly in cold-crystallized, cold-drawn PET [15].

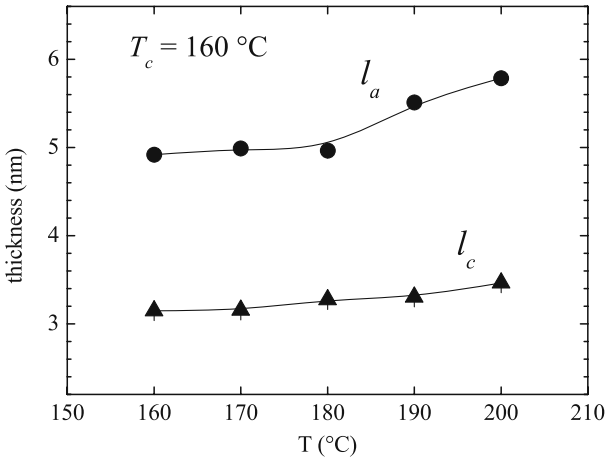

Fig. 3. Average layer thicknesses l_c and l_a computed from the SAXS data of the sample crystallized at 160 °C for 9 h, during a heating run at a rate of 2 °C/min. The lines are guides for the eye.

Once T_r is surpassed, the storage modulus E' decreases at a lower rate. This cannot be ascribed to an increase of crystallinity, following our SAXS and WAXS analyses shown below.

Figure 2 shows the WAXS crystallinity during a heating run at 2 °C/min (*i.e.* in the same conditions as the DMTA measurements) of samples crystallized at $T_c = 100$ and 160 °C. The inset of Figure 2 illustrates the coherence length D_{100} along the (100) direction for the same heating run. D_{100} was estimated from the integral breadth of the (100) reflection, as described in [5]. All data in Figure 2 are taken from our previous studies reported in reference [5]. Data for $T_c = 100$ °C will be discussed in the next subsection.

Figure 3 shows the average layer thicknesses l_c and l_a for $T_c = 160$ °C, derived from the IDF analysis of the

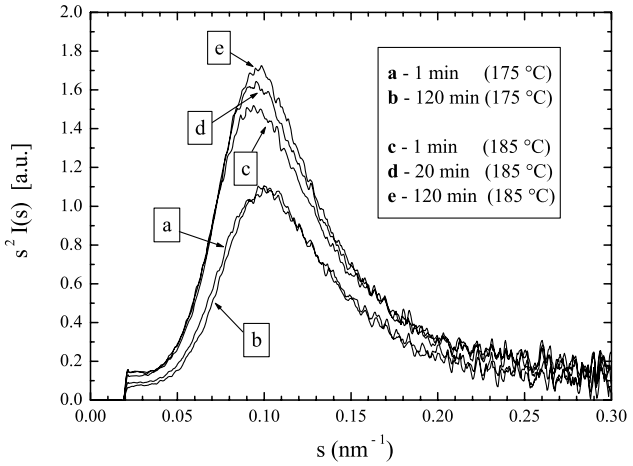

Fig. 4. Lorentz-corrected SAXS curves during isothermal measurements at 175 and 185 °C on the sample crystallized at 160 °C.

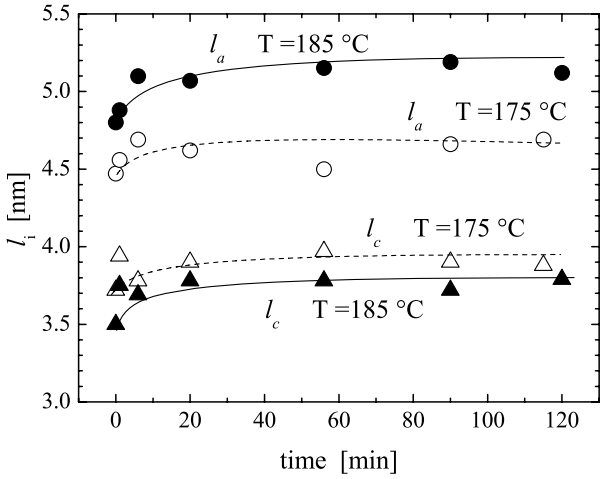

Fig. 5. Average lamellar and interlamellar thicknesses, l_c and l_a, respectively, derived from the IDF analysis of SAXS for the sample crystallized at 160 °C for 9 h, during isothermal experiments. The lines are guides for the eye.

SAXS patterns simultaneously recorded with the WAXS measurements of Figure 2.

For the high-T_c sample, the WAXS crystallinity always decreases during the heating run, while the linear crystallinity $\alpha_L \equiv l_c/(l_c + l_a)$ remains almost constant up to 180 °C, *i.e.* up to $\approx T_r$. The interesting point is that above T_r the linear crystallinity tends to decrease, the lamellar thickness l_c remaining almost constant. On the other hand, the slight increase of D_{100} observed within $T_c \leq T \leq 200$ °C could be associated to the perfecting of the lateral crystal packing. The sample weakening in the range $T_c \leq T \leq T_r$ (see Fig. 1) could be ascribed to the melting of either secondary crystals or imperfect lamellae, both grown *outside* the stacks (thus not visible by SAXS); the chains anchored to these lamellae would gain mobility upon crystal melting, thus contributing significantly to the drop of E'. The temperature T_r, however, represents a threshold for both the mechanical behavior and the (meta-) stability of the stacks.

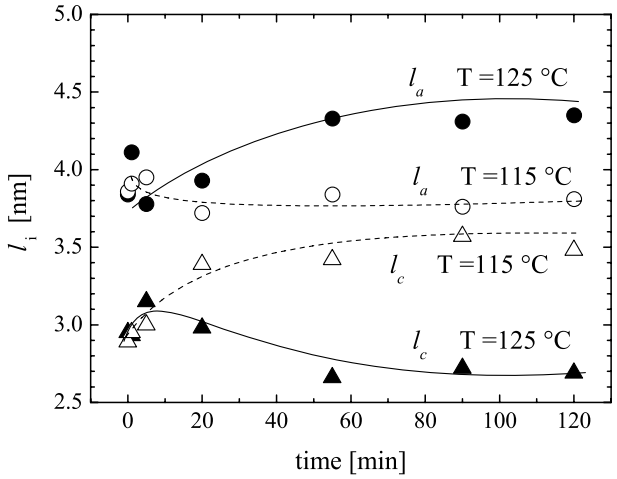

Fig. 6. Interface distribution function analysis of SAXS data obtained from the sample crystallized at 100 °C for 9 h, during subsequent isothermal experiments. The lines are guides for the eye.

In order to gain a deeper understanding on the nature of the structural rearrangements taking place at $T \approx T_r$, we carried out SAXS isothermal measurements on samples crystallized at 160 °C and further annealed at 175 and 185 °C, *i.e.* just below and above T_r. Figure 4 shows the Lorentz-corrected intensity, $s^2 I(s)$, observed from the two isothermal re-crystallization experiments. No significant changes in the pattern are visible during 2 h annealing at 175 °C, while at 185 °C, a change is observed as a function of time. The larger scattering power of the sample annealed at 185 °C is most probably related to changes in the density difference between the crystalline and the amorphous phases. The corresponding IDF results (see Fig. 5) show that l_c and l_a increase initially for both annealing temperatures, tending to stabilize after 20 minutes. Most interesting is the decrease in linear crystallinity when T increases from 175 to 185 °C, in agreement with the l_a increase shown in Figure 3.

3.2 Low-T_c sample

The DMTA, WAXS and SAXS data obtained upon heating the sample crystallized at $T_c = 100$ °C are significantly different from those of the high-T_c sample. Preceding calorimetric studies suggest that $T_r \approx 120$ °C for the low-T_c sample (see Ref. [14]). Thus we carried out two isothermal SAXS re-crystallization measurements at 115 and 125 °C.

Figure 6 shows the nano-structural evolution as revealed by the IDF analysis of the SAXS patterns of the low-T_c sample. In this case, the reaction of the system to a moderate heating above T_c (*i.e.*, $T = 115$ °C) is an increase of both the average lamellar thickness and the long period $L = l_c + l_a$ in the stacks, reaching a saturation level after ~ 50 min. However, when the isothermal exper-

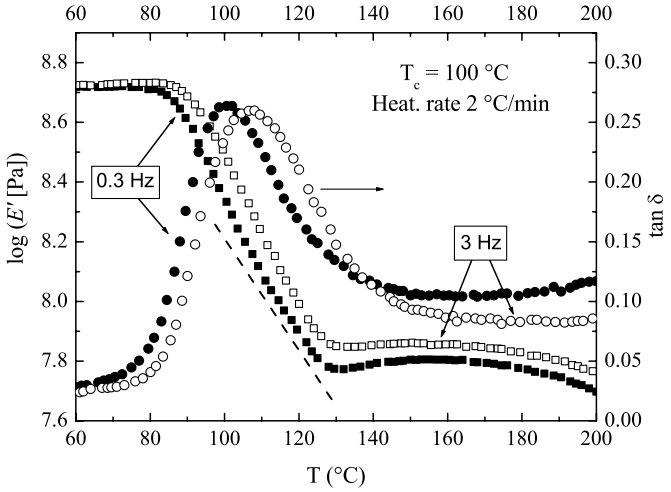

Fig. 7. Logarithm of the storage modulus E' at 0.3 and 3 Hz (left-hand axis) obtained with a heating rate of 2 °C/min on cold-crystallized PET annealed at the temperature T_c = 100 °C for 9 h. The corresponding loss tangent patterns are also reported (right-hand axis). The change of slope in the 0.3 Hz pattern of the storage modulus in the α region is highlighted by a straight dashed segment.

iment is carried out at the higher temperature of 125 °C, we observe a significant decrease of l_c down to a value surprisingly lower than that reached at 115 °C.

Additional information on the structural changes occurring upon heating the low-T_c sample can be drawn from Figure 2. Here, the WAXS crystallinity slightly decreases when heating up to 110 °C and then remains almost constant until T = 130 °C is reached. On the other hand, Figure 7 shows a slight decrease in the slope of the main α-relaxation just above the crystallization temperature (*i.e.*, at $\sim$ 110 °C). The strong influence of the α-relaxation itself impedes the accurate determination of the temperature where this change of slope takes place and simultaneously hides the details of the processes occurring just above T_c. Further above, at about 130 °C, the crystallinity increase leads to an enhancement in the elastic modulus.

In general, when the temperature T increases above T_c the lamellar stacks become less stable and some mechanism must set in to recover thermodynamic stability.

If the difference $T - T_c$ is relatively small ($\leq$ 15 °C), then the response of the stacks may be a partial melting (*i.e.* where some memory of the previous conformation still prevails) allowing for a change in structure and an increase of l_c. Another mechanism, which may accompany the former one, is the total melting of just the stacks in which the lamellae are thinner. This would explain the increase of l_c but not, of course, the mechanical behavior (*i.e.* the change of slope in Fig. 7 at $T \approx$ 110 °C). The amorphous regions left after the melting of the most unstable stacks, however, would be mobile enough to allow for a rapid re-crystallization into more stable structures (*i.e.* with larger l_c); this would account for a reduction in $|\mathrm{d}\log E'/\mathrm{d}T|$.

If, on the contrary, $T - T_c$ is sufficiently large ($\geq$ 25 °C), Figure 6 suggests that the new stability condition does not lead to a larger l_c value, but rather to larger interlamellar thicknesses l_a and to lamellae thinner than those formed at a lower temperature (*i.e.* at 115 °C). This circumstance seems to contrast with the general scheme outlined in references [16,17], where the heating of a structure formed in isothermal conditions is never accompanied by a decrease of l_c. However, we wish to point out that in the present case the structural rearrangement takes place when the interlamellar amorphous regions are still in a condition of a marginal glass, *i.e.* within the α-process dispersion region. For this reason the present situation differs quite significantly from those considered in references [16,17].

4 Thermodynamical aspects

Below the equilibrium melting point, the balance condition between the negative volume free-energy change and the positive basal surface energy contribution associated to the formation of a crystalline lamella leads to the definition of a thickness of marginal stability l_{c0} [18]

$$l_{c0} \simeq \frac{2\sigma_e}{\mu_a - \mu_c}\,, \tag{3}$$

where μ_a and μ_c are the segment chemical potentials in the amorphous and crystalline phases, respectively, and σ_e is the basal specific surface free energy. The stability threshold defined by equation (3) is indeed an important connection between morphological and thermodynamic properties in a semicrystalline system: lamellae of thickness lower than l_{c0} tend to melt; those with $l_c > l_{c0}$ tend to thicken spontaneously, this process being driven by the difference between volume and surface free-energy contributions.

In the initial stage of formation of a lamella, its thickness is somewhat larger than l_{c0} (to provide a finite thermodynamic force to grow), but once it has formed it will tend to either thicken or perfect or both, as described very clearly in [16,17]. It is then evident that the condition expressed by equation (3) cannot be of help in describing how and when the lamellar thickening process will come to an end. It is clear from the arguments outlined in the introductory section, that this process will slow down and asymptotically stop when certain thermodynamic conditions of the interlamellar amorphous layers are reached. This criterion will be discussed below.

Figure 8 illustrates the schematics of a lamella and its adjacent interlamellar layer. Let the chemical potentials in the crystalline bulk and in the interlamellar layer be μ_c and $\mu_a \equiv \mu_{a0} + \delta\mu_a$, respectively. The latter is expressed as the sum of two contributions: $\mu_{a0} \equiv \mu_{a0}(T)$ characterizes the amorphous domain in the absence of constraints; the other, $\delta\mu_a \equiv \delta\mu_a(T, L - l_c) > 0$ represents the effect of the constraints in the segmental fluctuation dynamics. Assuming $l_c > l_{c0}$ and a constant density (as an approximation), the change of the overall (specific) free energy associated to a variation δl_c of the lamellar thickness, for a fixed long period L, is

$$\delta F_{\mathrm{stab}} \simeq \left[\mu_c - (\mu_{a0} + \delta\mu_a)\right]\delta l_c + \left[\frac{\partial\delta\mu_a}{\partial l_c}\left(L - l_c + \frac{\partial\sigma_e}{\partial\delta\mu_a}\right)\right]\delta l_c. \tag{4}$$

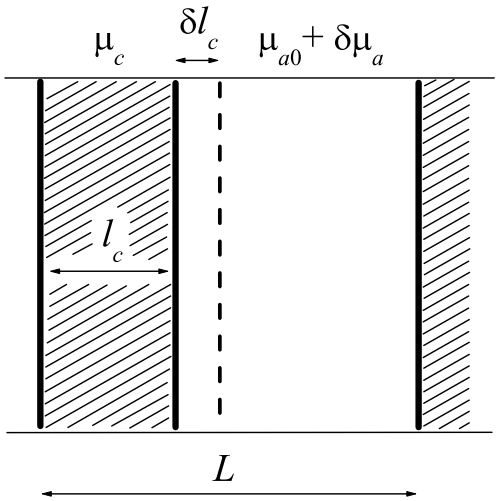

Fig. 8. Schematics of a lamella and an associated amorphous layer in a stack.

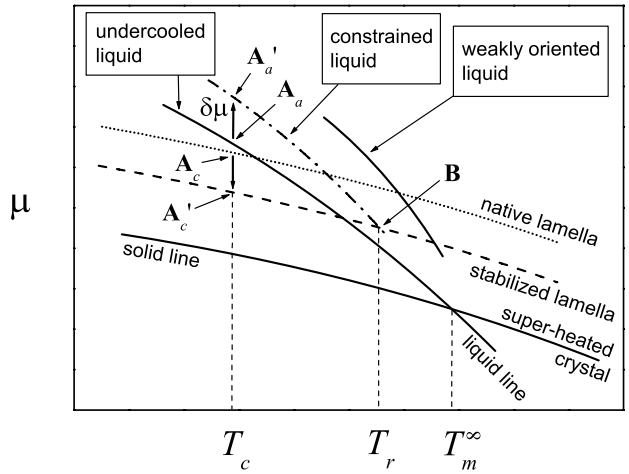

Fig. 9. Schematics of a phase diagram (chemical potential *vs.* temperature) describing the coexistence of amorphous and crystalline domains in a stack.

The first term on the right-hand side of equation (4) represents the decrease of the thermodynamic potential associated to the change of the segments from the constrained ($\delta\mu_a > 0$) amorphous state to the crystalline state. The second term consists of two parts, namely, i) the increase of $\delta\mu_a$ due to the reduction of $l_a = L - l_c$ (*i.e.* of the constraining volume) and ii) the variation of surface tension σ_e associated to the change of the chemical potential throughout the basal interphase. Equations similar in form to equation (4) have been used to discuss the reversible surface crystallization and melting in semicrystalline stacks of polyethylene ([19] and references therein). A finite $\delta F_{\rm stab} < 0$ represents the generalized thermodynamic force driving the thickening and/or the perfecting process. On the other hand, the criterion for structural stability is $\delta F_{\rm stab} = 0$; its practical implementation requires the explicit calculation of μ_a as a function of the constraining conditions and of the temperature, but this can only be done by means of a model (*e.g.*, the Gaussian chain model [2]; see also Ref. [19]).

After formation, a crystalline lamella tends to increase its thickness; in doing so, it imposes increasing constraints to the fluctuation dynamics in the inter-crystalline amorphous layer, which then becomes more rigid. This reduction of mobility contributes to the increase of the chemical potential μ_a. In order to further clarify the relationship between the physically intuitive increase of the mechanical performances of a stack and its thermodynamic description, let us consider the phase diagram depicted in Figure 9 (which is meant to describe the situation only from a qualitative point of view).

The (unconstrained) liquid line crosses the solid line at the equilibrium melting point T_m^∞. When a lamella forms at T_c, it is initially described by the *native* lamellar line (borrowing the nomenclature of Refs. [16] and [17]). This line is meant to represent an average chemical potential accounting for both the bulk crystalline and the surface contribution. The temperature where it intersects the liquid line is slightly larger than T_c: this guarantees that at T_c the native lamella is more stable than the (metastable) liquid and that it tends to grow (both laterally and in thickness). As times passes at T_c, the lamellar line shifts downwards; this is due to both thickening and perfecting. Simultaneously, this downward shift causes an increase $\delta\mu_a$ of the chemical potential in the amorphous interlamellar regions, with respect to the value $\mu_{a0}(T_c)$. This process leads to the drift of point $\mathbf{A}_a$ (the chemical potential of the liquid at T_c) towards $\mathbf{A}'_a$ (constrained liquid at T_c) and of point $\mathbf{A}_c$ (the chemical potential of the native lamella at T_c) towards $\mathbf{A}'_c$ (stabilized lamella at T_c), until the condition $\delta F_{\rm stab} = 0$ is reached (see Fig. 9).

Note that in the new state (*i.e.* constrained liquid and stabilized lamellar lines) the temperature at which lamellae reach instability has shifted to $T_r > T_c$ (point **B** of Fig. 9). Hence, in this scheme, perfecting is responsible of the progressive drift with annealing time of the temperature T_r where the first endotherm is observed in DSC experiments (cf., for instance, Ref. [14]). Of course, this is a relatively slow process, as its rate is controlled by the occurrence of conformational fluctuations with free energy ΔF (cf. Eq. (1)), whose probability $p \propto \exp\{-\Delta F/k_{\rm B}T\}$ may be very small (see, for instance, [3]) and in general decreases with time because progressive perfecting is accompanied by a slight increase of the free-energy barrier ΔF.

5 Discussion

5.1 The hypothesis of local chain orientation

Let us focus our attention on the sample crystallized at 160 °C. When T_r is crossed upon heating ($\approx$ 180 °C), a structural rearrangement sets in, as is clearly seen by SAXS (see Figs. 3 and 4). The IDF analysis suggests that this rearrangement does not involve a significant crystal thickening; rather an interlamellar thickening. This is a clear indication that the thermodynamic properties of the amorphous phase have changed. We suggest that a partial

average orientation of the chains within the interlamellar regions develops, in a direction almost perpendicular to the basal planes. The following reasons support this contention:

1) Local chain orientation is a precursor of crystallization; hence, if during the structural rearrangement of the system a state of lower overall free energy is reached (just above T_r), the system itself will settle in it even if it is metastable.
2) The gradient of chain conformational entropy contributes to the surface tension. This gradient is lower in the transition from bulk crystalline to a partially oriented phase than in that from the crystal to a less oriented phase. An analogous role is played by the mesophase in the model put forward in references [16, 17]: the surface tension associated to a lamella surrounded by the mesophase is lower than in the case where the lamella is surrounded by an ordinary amorphous phase (see Eqs. (9) and (10) of Ref. [17]).
3) The reduction of the chain orientational entropy in the transition to a partially oriented conformation contributes with a positive term in $\delta\mu_a$.
4) The above items 2) and 3) are in favour of a reduction of the instability threshold l_{c0} expressed by equation (3), in such a way that just above T_r the lamellae that were unstable at the temperature of structural rearrangement now become more stable, even if maintaining the same thickness.
5) The density autocorrelation length ξ in an aligned amorphous phase is larger (along the orientation direction) than in an isotropic phase; this implies that the aligned phase may exhibit glassy behaviour (*i.e.* a constrained dynamics) at a temperature higher than the corresponding unoriented phase [2].
6) Due to the increase of ξ, the effect of chain pinning to the basal planes of adjacent lamellae increases as well, leading to an enhancement of the mechanical performances of the amorphous interlamellar region (see Fig. 1 and the DMTA results of Ref. [2]).

The new, partially oriented, amorphous state is represented in Figure 9 as a liquid line which is shifted upward with respect to the ordinary liquid one ("weakly oriented liquid" line). The items listed above describe in fact the character of what may be called a Rigid Amorphous Phase (RAP). In particular, item 3) above is a statement about the stabilizing effect of the RAP on the crystalline lamellae.

5.2 Constraining conditions from statistical mechanics

The influence of mean chain orientation on the excess chemical potential $\delta\mu_a$, for given constraining conditions on the density fluctuations, has been estimated in reference [2] within the framework of the Gaussian chain approximation [1]. Here we only recall the relevant definitions and the final result of the calculations.

The degree of chain orientation is described by an orientation parameter, κ, which describes the chain conformation through the probability distribution $\psi \equiv \exp\{-(3/2a^2)\int_0^n \mathrm{d}\tau\,[\dot{\mathbf{r}}_\perp^2 + \kappa^{-1}\dot{\mathbf{r}}_\parallel^2]\}$, where a is the length of a statistical segment and n is proportional to the degree of polymerization. An isotropic chain is described by $\kappa = 1$, whereas $\kappa > 1$ gives a larger probability for the segment to be oriented along the direction labelled by a "$\parallel$".

On the other hand, the constraining conditions are accounted for by setting a lower bound, $k_a \equiv 2\pi/l_a$, to the component perpendicular to the basal planes of the wave vectors associated to the density normal modes quenched due to confinement.

As a final result, the difference $\Delta(\delta\mu_a) \equiv \delta\mu_a(\kappa) - \delta\mu_a(\kappa = 1)$ can be expressed as a function of T and ξ_0 (the density autocorrelation length for an isotropic melt in the absence of constraints) by the following relation:

$$\Delta(\delta\mu_a) \simeq k_\mathrm{B}T\frac{av}{\pi^2}\left\{k_a \ln\left(\frac{\kappa\Lambda^2+1}{\Lambda^2+1}\right) - \frac{2}{\xi_0}\left[\kappa^{-1/2}\arctan(\Lambda\kappa^{1/2}) - \arctan(\Lambda)\right]\right\}, \quad (5)$$

where $\Lambda \equiv \xi_0 k_a$ and $v \equiv v_0(1 - \Theta/T)$ is the interaction parameter, with v_0 and Θ constants. The density autocorrelation length ξ_0 is related to the average segment number density c by $\xi_0 = (8avc)^{-1/2}$. On the other hand, the density autocorrelation length along the orientation direction, ξ, in a melt without confinement, is given by $\xi = \sqrt{\kappa}\xi_0$.

5.3 High-T_c sample: influence of amorphous constraining

It is possible to evaluate an upper limit for the *change* of the excess chemical potential $\delta\mu_a$ across the transition at T_r by assuming that the lamellae are very close to their stability limit (Eq. (3)) just below the transition temperature, *i.e.* at $T_1 \equiv 175\,^\circ$C, as well as at $T_2 \equiv 185\,^\circ$C. Indeed, at T_1 the lamellae are just about to lose their stability; on the other hand, Figure 4 clearly shows that, during at least the first 2 h, the structures formed at $T = T_2$ drift towards a different condition, which allows us to consider the lamellae as only marginally stable. These assumptions, together with the constancy of l_c across the transition revealed by the IDF analysis of Figure 3, imply the following relation between the variations of σ_e, $\delta\mu_a$ and the difference $\mu_{a0} - \mu_c$:

$$\Delta \ln \sigma_e = \Delta \ln(\mu_{a0} - \mu_c + \delta\mu_a). \quad (6)$$

Now, the experimental results reported above support the hypothesis that the amorphous fraction becomes more constrained after crossing T_r, that is, $\Delta(\delta\mu_a) \equiv \delta\mu_a|_{T_2} - \delta\mu_a|_{T_1} > 0$. On the other hand, in the hypothesis that $\Delta\sigma_e \leq 0$, we conclude that

$$\Delta(\mu_{a0} - \mu_c + \delta\mu_a) \leq 0, \quad (7)$$

the equality holding in the case that $\Delta\sigma_e = 0$ (an assumption that has already been adopted in the calculations

presented in Ref. [2]). Since

$$\mu_{a0} - \mu_c \cong \frac{H_f(T_m^\infty - T)}{T_m^\infty}\,, \tag{8}$$

with the enthalpy of fusion $H_f \simeq 25\,\mathrm{kJ/mol}$ and the melting temperature $T_m^\infty \simeq 285\,^\circ\mathrm{C}$ [20], we find $\Delta(\delta\mu_a) \approx 0.45\,\mathrm{kJ/mol}$ as an upper limit.

Assuming a equal to the contour length of three monomers (*i.e.* twice the persistence length, which has been estimated to be around 1.4 nm [21]), a density correlation length $\xi \simeq 1\,\mathrm{nm}$ [22], $\kappa|_{T_1} = 1$, and a segment number density $c \simeq 4.3\,\mathrm{nm}^{-3}$, we see that the above estimated value of $\Delta(\delta\mu_a)$ can be obtained by setting $\kappa|_{T_2} \simeq 2$ in equation (5).

5.4 Low-T_c sample: effect of a marginal glassy state

Let us recall first the phase diagram of Figure 9. The slopes of both the weakly oriented liquid and the constrained liquid lines are slightly larger than that of the ordinary liquid. This would apparently contradict the Gibbs-Duhem relation

$$\frac{\partial \mu}{\partial T} = -s, \tag{9}$$

where s (not to be confused with the scattering vector of Fig. 4) is the specific entropy: a constrained liquid (*i.e.* less entropic) would apparently have a specific entropy larger than the unconstrained liquid. This apparent contradiction is a consequence of the application of thermodynamics (Eq. (9)) to non-equilibrium states where kinetic processes play a fundamental role. Indeed, the new liquid line represents to a certain extent a marginal glass: when the temperature rises, an ever increasing number of fluctuational degrees of freedom defreeze (because ξ decreases upon increasing T [2]); this leads to an apparent faster decrease of μ_a, which of course has no meaning in a strict thermodynamic sense. It is noteworthy that a consequence of this mechanism is the apparent depression of the melting point extrapolated by means of a Gibbs-Thomson representation in a system where lamellar thickening is hindered by the vitrification of the interlamellar regions [2]. The observation that a marginal glass may show an apparent entropy larger than its defrozen liquid will help in the discussion of the low-T_c case.

We now turn to the discussion of the experimental results. The DMTA pattern of the sample crystallized at 100 °C (Fig. 7) suggests that the structural rearrangements (revealed by the IDF analysis of Fig. 6) start already when the α-relaxation has not yet come to completion and hence when the amorphous phase still exhibits a limited mobility. As T is raised, the density fluctuation modes with lower wavelength, among the frozen ones, defreeze first; in the present case, still a rather large fraction of long-wavelength density modes remain quenched when rearrangement starts.

Due to lamellar perfecting at 100 °C, the resulting constrained liquid line is (locally) much steeper than in the case of $T_c = 160\,^\circ\mathrm{C}$ because at this low temperature the glassy character of the amorphous regions is enhanced. Upon increasing T above the threshold from which structural rearrangement starts, the amorphous interlamellar regions rapidly gain mobility, but the long-wavelength modes, that have to be necessarily involved in the conformational transition leading to a partially oriented liquid, are still inactive. For this reason, only the crystalline lamellae that reach a larger thickness would stabilize, that is, by a downward shift of the lamellar line in the phase diagram of Figure 9. This would explain the l_c increase observed at 115 °C as a function of time (see Fig. 6). Upon further heating at $T > T_r$, the relevant density modes, able to lead to a large-scale partial chain orientation, are now defrozen. This allows for the development of a partially oriented amorphous phase which tends to stabilize the lamellae in a similar way as that described for the high-T_c sample above T_r. As a consequence, the new stability threshold, l_{c0}, becomes lower and lamellae with smaller thickness are now stable (in other words, the *effective* liquid line has now shifted upward; this fact can be considered the stabilizing effect of the RAP). The results shown in Figure 6 (for $T = 125\,^\circ\mathrm{C}$) support this interpretation. We cannot go into details about the causes which lead to the stacks' instability at $T_r \sim 120\,^\circ\mathrm{C}$ (the limit to the increase of lamellar thickness may be related to a maximum possible density of conformational defects trapped within the interlamellar regions, to cite an example), but at the end, this instability will show up and a melting of the stacks will take place, initiating the restructuring process.

Let us estimate the excess chemical potential change $\Delta(\delta\mu_a)$ involved in the structural reorganization of the low-T_c crystallized sample. We first assume that σ_e remains constant when passing from the state reached at 115 °C to the final one at 125 °C. Since the temperature in both of these states lies within the glassy region of the interlamellar amorphous phase (*i.e.* $90\,^\circ\mathrm{C} \leq T \leq 150\,^\circ\mathrm{C}$, cf. Refs. [2,15] and Fig. 1), we may consider the latter always in a state of marginal glass, with which the lamellae are in equilibrium. At $T = 115\,^\circ\mathrm{C}$ the excess chemical potential is $\delta\mu_a|_{\kappa=1}$, while at $T = 125\,^\circ\mathrm{C}$ (*i.e.* in the more oriented glassy state) the excess chemical potential is $\delta\mu_a|_{\kappa>1} > \delta\mu_a|_{\kappa=1}$. In addition, we consider that in both cases the lamellar thicknesses are close to the stability limit expressed by equation (3), where $\mu_a = \mu_{a0} + \delta\mu_a|_{\kappa=1}$ or $\mu_a = \mu_{a0} + \delta\mu_a|_{\kappa>1}$ depending on the state. Finally, we find the following approximate expression:

$$\begin{aligned}\Delta(\delta\mu_a) &\equiv \delta\mu_a|_{\kappa>1} - \delta\mu_a|_{\kappa=1} \\ &\approx (\mu_{a0} - \mu_c)\left[\frac{(l_{c0})_{T=125\,^\circ\mathrm{C}}}{(l_{c0})_{T=115\,^\circ\mathrm{C}}} - 1\right].\end{aligned} \tag{10}$$

Using equation (8), the literature data for H_f and T_m^∞ of PET [20] and the l_a values at long times in Figure 6, we obtain $\Delta(\delta\mu_a) \approx 2\,\mathrm{kJ/mol}$. Application of equation (5) to this case yields $\kappa \simeq 8$, a value which seems to be somehow overestimated. Nevertheless, this numerical result is satisfactory, given the approximate character of our model, and indeed suggests that κ increases across T_r, *i.e.*, orientational effects in the interlamellar regions cannot be disregarded.

6 Conclusions

The central point addressed in this paper is the necessity to consider the evolution of the thermodynamic state of the amorphous domains as an essential aspect accompanying the crystal growth in polymers. Lamellar crystal structures cannot be considered thermodynamic subsystems interacting with an invariable environment. In this respect, considering the whole lamellar stack as a subsystem, with both its crystalline and amorphous components, is a better suited choice for a comprehensive understanding of the crystallization process at a coarse grained level (a similar point of view has been put forward also in Ref. [23], although from a different approach). The application of this idea to the re-crystallization of PET, with its evident peculiarities, leads quite naturally to the necessity of the existence of amorphous domains where the segmental mobility is depressed. They possibly represent just a subset of a more general class of rigid amorphous domains.

The Rigid Amorphous Phase has had a central role in the interpretation of a number of experimental observations [24–26], but to our knowledge this is the first time that it is envisaged to influence the lamellar stacks structuring in the re-crystallization process. The development of a RAP has been shown to be intimately connected with the formation of the crystals (see also Refs. [9,26]). In the present study, the RAP appears to yield a stabilizing effect on the crystalline lamellae also in the structural reorganization process taking place above the crystallization temperature. In this sense, it can be defined as a *parasitic phase* and probably this is the reason why it encounters great difficulties to be described thermodynamically, in contrast to other phases whose character is less influenced by interfacial effects.

Despite this, we attempted to offer a description of the RAP in terms of statistical mechanical concepts. Within the limits inherent to the nature of the models we used (see Ref. [2]), we hope that the point of view developed in this study will be a useful hint for a further progress in this field.

The authors gratefully acknowledge the Ministerio de Educación y Ciencia (Grant No. FIS2004-01331), Spain, for the financial support of this investigation. F.J.B.C. also wishes to acknowledge the Alexander von Humboldt Foundation for the generous support during this work. The experimental work carried out at HASYLAB, DESY, Hamburg, was supported by the European Community Research Infrastructure Action under the FP6 "Structuring the European Research Area" Programme (project II-07-031 EC). Thanks are also due to S.S. Funari and M. Dommach for their technical support at DESY beamline A2. M.P. gratefully acknowledges MCYT for the award of a sabbatical grant (SAB-2006-0077) to work at IEM, CSIC, Madrid and CNR, Italy, for supporting this initiative within the framework "Congedi per Motivi di Studio". M.P. is also grateful to Prof. G. Strobl for his kind invitation to the Physikalisches Institut, Albert-Ludwigs-Universität Freiburg and for the useful discussions.

References

1. M. Doi, S.F. Edwards, *The Theory of Polymer Dynamics* (Oxford University Press, Oxford, 1998).
2. F.J. Baltá Calleja, A. Flores, G. Di Marco, M. Pieruccini, Phys. Rev. B **75**, 224201 (2007).
3. M. Pieruccini, T.A. Ezquerra, M. Lanza, J. Chem. Phys. **127**, 104903 (2007).
4. G. Adam, J.H. Gibbs, J. Chem. Phys. **43**, 139 (1965).
5. A. Flores, M. Pieruccini, U. Nöchel, N. Stribeck, F.J. Baltá Calleja, Polymer **49**, 965 (2008).
6. R.K. Verma, B.S. Hsiao, Trends Polym. Sci. **4**, 312 (1996).
7. A.A. Minakov, D.A. Mordvintsev, C. Schick, Polymer **45**, 3755 (2004).
8. B. Wunderlich, Progr. Polym. Sci. **28**, 383 (2003).
9. R. Androsch, B. Wunderlich, Polymer **46**, 12556 (2005).
10. W. Ruland, Colloid Polym. Sci. **255**, 417 (1977).
11. N. Stribeck, Colloid Polym. Sci. **280**, 254 (2002).
12. J.J. Hermans, Rec. Trav. Chim. Pais-Bas **63**, 211 (1944).
13. N. Stribeck, *X-ray Scattering of Soft Matter* (Springer, Heidelberg 2007) p. 179.
14. G.C. Alfonso, E. Pedemonte, L. Ponzetti, Polymer **20**, 104 (1979).
15. A. Bartolotta, G. Di Marco, F. Farsaci, M. Lanza, M. Pieruccini, Polymer **44**, 5771 (2003).
16. G. Strobl, Prog. Polym. Sci. **31**, 398 (2006).
17. G. Strobl, T.Y. Cho, Eur. Phys. J. E **23**, 55 (2007).
18. M. Pieruccini, G. Di Marco, M. Lanza, J. Appl. Phys. **80**, 1851 (1996).
19. T. Albrecht, G. Strobl, Macromolecules **28**, 5827 (1995).
20. J. Brandrup, E.H. Immergut, E.A. Grulke (Editors), *Polymer Handbook*, 4th edition (Wiley, New York, 1999).
21. M. Imai, K. Kaji, T. Kanaya, Y. Sakai, Physica B **213, 214**, 718 (1995).
22. C. Schick, E. Donth, Phys. Scr. **43**, 423 (1991).
23. T.Y. Cho, B. Heck, G. Strobl, Chin. J. Polym. Sci. **25**, 83 (2007).
24. V.B.F. Mathot, *Thermal characterization of states of matter*, in *Calorimetry and Thermal Analysis of Polymers*, edited by V.B.F. Mathot (Hanser, Munich, 1994) p. 105.
25. M. Kattan, E. Dargent, J. Grenet, Polymer **43**, 1399 (2002).
26. C. Schick, A. Wurm, A. Mohamed, Colloid Polym. Sci. **279**, 800 (2001).